Nanocomposites of isotactic polypropylene with carbon nanoparticles exhibiting enhanced stiffness, thermal stability and gas barrier properties

A. Vassiliou, D. Bikiaris, K. Chrissafis, K.M. Paraskevopoulos, S.Y. Stavrev, A. Docoslis

Nanocomposites of isotactic polypropylene with carbon nanoparticles exhibiting enhanced stiffness, thermal stability and gas barrier properties

A. Vassiliou, D. Bikiaris, K. Chrissafis, K.M. Paraskevopoulos, S.Y. Stavrev, A. Docoslis

PII: S0266-3538(07)00315-6
DOI: 10.1016/j.compscitech.2007.08.019
Reference: CSTE 3796

To appear in: *Composites Science and Technology*

Received Date: 30 May 2007
Revised Date: 25 July 2007
Accepted Date: 10 August 2007

Please cite this article as: Vassiliou, A., Bikiaris, D., Chrissafis, K., Paraskevopoulos, K.M., Stavrev, S.Y., Docoslis, A., Nanocomposites of isotactic polypropylene with carbon nanoparticles exhibiting enhanced stiffness, thermal stability and gas barrier properties, *Composites Science and Technology* (2007), doi: 10.1016/j.compscitech.2007.08.019

Nanocomposites of isotactic polypropylene with carbon nanoparticles exhibiting enhanced stiffness, thermal stability and gas barrier properties

A. Vassiliou[1], D. Bikiaris[1*], K. Chrissafis[2], K. M. Paraskevopoulos[2], S.Y. Stavrev[3] and A. Docoslis[4]

[1]Laboratory of Organic Chemical Technology, Department of Chemistry, Aristotle University of Thessaloniki, GR-541 24 Thessaloniki, Macedonia, Greece.
[2] Solid State Physics Section, Physics Department, Aristotle University of Thessaloniki, GR- 541 24, Thessaloniki, Macedonia, Greece.
[3] Bulgarian Academy of Sciences, Space Research Institute, Department of Space Materials and Nanotechnologies, 6 Moskovska St, Sofia Bulgaria.
[4]Department of Chemical Engineering, Queen's University at Kingston, Kingston, ON Canada K7L 3N6.

Abstract

Carbon nanoparticles (CN), synthesized by a shock wave propagation method from the free carbon of the explosive, were dispersed in isotactic polypropylene (iPP) using a twin screw co-rotating extruder. These materials were analyzed for their tensile properties, crystallization morphology, thermal stability under N_2, O_2 and air, as well as their permeability rates for N_2, O_2 and CO_2. Young's modulus was significantly enhanced, as was the tensile strength at the yield point, although at a smaller extent. However, the tensile strength and elongation at the break point slightly deteriorated with the increase of the filler's concentration. This behavior was attributed to the increase tendency of CN to form aggregates into iPP matrix by increasing its content. The size of aggregates, as was evaluated by extended micro-Raman mapping, is ranged from 1 up to 5 μm. The nanoparticles caused a significant reduction of the iPP chain's mobility leading to smaller and less ordered crystallites, with the appearance of γ-phase crystallites at CN content 5 wt%. In inert atmosphere (N_2) the presence of the nanoparticles caused a shift of the starting decomposition temperature (T_d), from 368 up to 418.6^{o}C, while, under oxygen, thermal decomposition was more complex, displaying more than two stages. The T_d was slightly lowered, up to a filler content of 2.5 wt%, with the nanoparticles exhibiting a catalytic role at the beginning of the polymer's decomposition. Under air, the degradation behavior was between

those exhibited in inert and O_2 atmospheres. Permeability rates for the gases measured were substantially lowered with increasing filler content.

Keywords: A. Nanocomposites; A. Carbon nanoparticles; B. Mechanical properties; B. Thermal properties; D. Raman spectroscopy.

* Corresponding author. Tel.: +30 2310 997812; fax: +30 2310 997667.

E-mail address: dbic@chem.auth.gr

1. Introduction

Carbon black (*CB*) additives are extensively used in rubber and plastic products as fillers, reinforcing agents and pigments [1]. Their most common usage (~70 %) is as a pigment and reinforcing phase in automobile tires. Carbon black helps conduct heat away, reducing thermal damage, and increasing tire life. Carbon black is practically used in all rubber products (hence their acquired black colour) where tensile and abrasion wear properties are crucial. In rubber products where other colours are desired, precipitated or fumed silica is used. Furthermore, carbon blacks enhance *UV* stability, electrical conductivity and mechanical properties or weather resistance of plastics [2]. The propensity to agglomeration of primary spherical particles of carbon black results in the appearance of a spatial network in the polymer, with aggregates behaving like fibrous fillers. This causes a increase of electrical resistance even for a small content of carbon black [3, 4]. To a large extent carbon black is used in polyethylene pipelines to enhance their weathering performance and thermo-oxidative stability, and in polypropylene geotextiles applied for soil reinforcement, filtration, and other construction purposes. Finally, activated carbon black is used extensively nowadays as a reheating agents for the production of carbonated soft drink bottles composed from poly(ethylene terephthalate) (PET) [5].

All carbon blacks are produced by partial combustion of liquid or gaseous hydrocarbons and have chemisorbed oxygen complexes (carboxylic, quinonic, lactonic, phenolic, etc.) on their surface to varying degrees, depending on the specific manufacturing conditions. The sum of all these groups is usually referred to as its volatile content and directly affects the properties of the material. Due to its chemical structure and physical properties, carbon blacks usually exhibit a stabilizing effect in composites. Its polyaromatic structure, containing mainly hydroxyl, carboxyl and quinone groups, is prone to the absorption of UV radiation [6]. Carbon blacks also act as

quenchers of excited states, acceptors of free radical species [7] and hydroperoxide decomposers [6]. Moreover, the thermal stability of the polymer can be either improved or deteriorated, depending whether the volatile content is high or low, respectively [8]. The extent of the aforementioned interactions in composites is usually related to the particle size of the carbon black, as well as to the concentration and dispersion degree in the polymer matrix [9].

Isotactic polypropylene (iPP) is probably one of the most interesting commodity thermoplastic accounting for about 20 % of the total world polyolefins production [10], not only for its balance of physical and mechanical properties, but also due to its environmental friendliness (recyclability) and low cost. It is widely used in many applications, such as fibers, films for food packaging, bottles production, tubes, etc., gradually replacing other traditionally used polymers, such as polyvinylchloride (PVC) and polystyrene (PS), in many of their applications. In recent years there is also an interest to enhance some of their properties by adding small amounts of nanoparticles. Polypropylene filled with carbon black additives, after a critical CB loading, known as the percolation concentration, conducts electricity. Above percolation concentration most mechanical properties, such as tensile and impact strength, are reduced, remaining nonetheless satisfactory for many applications [5]. Furthermore, although additives immiscible with polymers, such as carbon black, are mostly distributed in the amorphous phase their impact on the formation of the crystalline structure is significant [11]. However, in all above applications, carbon black is used in the form of microparticles and, generally, there is lack of scientific work concerning the use of carbon black nanoparticles (CN).

Polymer nanocomposites are a relative new class of hybrid materials, composed of an organic polymer matrix impregnated with materials having at least one of their dimensions in the nanometer range [12]. Compared to conventional composites, polymer nanocomposites exhibit a much increased internal interfacial area, resulting in maximized polymer-nanoparticles interactions, since the filler is dispersed on a nanometer scale. Most products require a balance between stiffness and impact strength, and this need has been met using several nanoparticles, at loadings of 10% or less, increasing the range of the material's applications [13-15]. Although nanocomposites can be prepared either through melt compounding [16-20] solution blending [21], in situ polymerization techniques [22, 23] and sol-gel reactions [24], due to its compatibility with current industrial processes, such as extrusion and injection molding, the absence of organic solvents, and its suitability with most commodity polymers, melt-mixing is

probably the most industrially feasible and versatile technique amongst the various strategies used for the preparation of nanocomposites.

The aim of the present study is to prepare iPP/CN nanocomposites by using carbon black nanoparticles synthesized by a relatively new method [25], in order to evaluate their effect on mechanical properties, crystallization, thermal stability and permeability rates of iPP matrix.

2. Experimental

2.1. Materials

The carbon nanoparticles (CN) used in this study were synthesized by a shock wave propagation method from the free carbon of the explosive [25]. Using optimal synthesis conditions (pressure, time, temperature), carbon nanoparticles with controlled size and content were obtained. They consisted of disordered graphite (67 wt%) and diamond (33 wt%), and had a mean diameter of 1-3 nm, a specific surface of 590 m^2/g (*BET*) and a specific gravity of 1.86 g/cm^3. Isotactic polypropylene was supplied by Basell Polyolefines and had a melt flow index (*MFI*) of 12 g/10 min at 190 ^oC, T_m 162.1 ^oC and a degree of crystallinity 62.8 %.

2.2. Nanocomposites preparation

Nanocomposites containing 0.25, 0.5, 0.75, 1, 2.5 and 5 wt % CN nanoparticles were prepared by melt mixing in a Brabender (model *DSC Φ25/32D*) twin screw co-rotating extruder with L/D 32 (D25 mm). Along the screw there were different screw elements [13] in order to induce polymer melting and achieve fine dispersion of the nanoparticles in the polymer melt. Prior to melt processing, carbon nanoparticles were dried for 24 h at 140^oC. Compounding was carried out using a screw rotating speed of 225 rpm and also a temperature profile 175, 180, 185, 190, 190, 195, 190 ^oC at the sequential heating zones, from the hopper to the die. After compounding, the material was extruded from a die which had three cylindrical nozzles of 4 mm diameter, to produce cylindrical extrudates. These were immediately immersed in a cold-water bath (20 ^oC) and palletized.

2.3. Mechanical properties

Measurements of the mechanical properties, such as tensile strength and elongation at break, were performed on an Instron 3344 dynamometer, in accordance with ASTM D638 using a

crosshead speed of 50 mm/min. At least five measurements were conducted for each sample, and the results were averaged to obtain a mean value. The specimens were prepared in a single screw injection machine by Engel (Monomat 80, Germany) containing three different heating zones. The temperatures of each zone were 245/195/190^{o}C respectively, from the feeding zone to the die, while the mold was cooled with water at 20^{o}C.

2.4. Transmission electron microscopy (TEM).

Electron diffraction (ED) and Transmission Electron microscopy (TEM) investigations were made on ultra thin film samples of the various nanocomposites prepared by an ultra-microtome. These thin films were deposited on copper grids. ED patterns and TEM micrographs were obtained using a JEOL 120 CX microscope operating at 120 kV.

2.5. Micro-Raman Spectroscopy

Raman studies of the iPP/CN samples were performed by using a Jobin-Yvon/Horiba micro-Raman Spectrometer (Model: Labram) with spectrum resolution capability 3-4 cm^{-1}, equipped with a 632 nm He/Ne laser source, 1800 1/nm grating and an Olympus BX41 microscope system. Collection of the spectra was performed at room temperature under the following conditions: x100 microscope objective, 100μm pinhole size, 300 μm slit width. Exposure times and laser powers in the range 20-120 s and 3-30 mW, respectively, were used. At CN concentrations above 0.5 wt%, attenuating filters were used for the laser beam in order to avoid excessive sample heating and the exposure times were adjusted accordingly. Each spectrum represents the average of two measurements. Sample profiling (2D mapping) was performed under the same conditions at a step increment of 0.5 μm in both x- and y-direction.

2.6. Polarizing Optical Microscope (POM)

Microscopic observations of morphological features and changes during crystallization of iPP/CN nanocomposites were carried out using a polarizing optical microscope (Nikon, Optiphot-2) equipped with a Linkam *THMS* 600 heating stage, a Linkam TP 91 control unit and also a Jenoptic ProgRes C10plus camera with the Capture Pro 2.1 software.

2.7. Wide-angle X-ray Diffractometry (WAXD)

WAXD study of iPP/CN nanocomposites was performed over the range 2θ from 5 to 55°, at steps of 0.05° and counting time 5 sec, using a Philips PW1710 powder diffractometer, with CuK_α Nickel-filtered radiation.

2.8. Thermal analysis

Thermogravimetric analysis was carried out with a SETARAM SETSYS TG-DTA 1750 °C system. Samples (11.0 ± 0.5 mg) were placed in alumina crucibles. An empty alumina crucible was used as reference. iPP/CN nanocomposites were heated from ambient temperature to 500 °C in a 50 ml/min flow of N_2, O_2 and dry air at a heating rate of 10 °C/min. Continuous recordings of sample temperature, sample weight, its first derivative and heat flow were received.

2.9. Permeability studies.

Permeability rates were studied on relatively thin films (50 ± 5 μm) of iPP/CN nanocomposites, which were prepared by an Otto Weber, Type PW 30 hydraulic press connected with an Omron E5AX Temperature Controller, at a temperature of 190 ± 5°C under a load of 10 kN on a ram of 110 mm followed by quenching in cold water (20 °C). Permeability rates of O_2, N_2 and CO_2 through these films were measured using a Davenport Apparatus (London). From each sample 3 measurements were conducted and the results were averaged to obtain a mean value.

3. Result and Discussion

3.1 Mechanical properties

The stress-strain curves of all the prepared materials were comparable to that of neat iPP, thus classified as hard and tough materials. Neck formation appeared at the yield point for all nanocomposites. However, only for concentrations up to 0.25 wt% CN, the stress at break value was higher than at the yield point, and yielding was observed as the predominant deformation mechanism. For higher filler concentrations the tensile stress at the break point was lower than at the yield point and brittle fractures occurred. The stress at the yield point values (Figure 1) revealed that, for the range studied, there is a small increase with filler content. A maximum improvement of 14 % was found for CN concentration of 5 wt%. Tensile stress at the yield point depends mainly on the microstructure, including interfacial bonding, as well as the form and size

distribution of the filler, its spatial distribution in the matrix and the thickness of the interface. Poor bonding between matrix and filler result in a brittle material, due to the fact that the applied load is not effectively transferred to the filler. When tensile stress at the break point is lower than at the yield point a brittle fracture occurs. Yielding will occur when the opposite holds true. For some bonding between matrix and filler Turcsányi et al. proposed an equation to predict the extent of interfacial adhesion [26]. A constant *B* is introduced, which, although it does not have any direct physical meaning, it is related to the interfacial properties of the particular system, and also depends on the yield stress of the matrix. When *B* is higher than 3 interfacial bonding is enhanced with increasing volume fraction. The equation proposed is as follows:

$$\sigma_{yc} = [(1-\Phi)/(1+2{,}5\Phi)]\ \sigma_{ym}\ e^{B\,\Phi} \qquad (1)$$

where, Φ is the volume fraction of the filler and σ_{yc}, σ_{ym} are the yield stresses of the composite and matrix, respectively. Up to a CN concentration of 1 wt% a significant jump is observed, revealing a very strong interfacial bonding. Turcsányi's equation is not able to predict this jump, since *B* would be forced to take unrealistic high values. However, for higher concentrations the increase is smoothened and follows the trend predicted for *B* = 6. Thus, it can be concluded that there is a significant amount of cohesion between the polymeric matrix and the carbon nanoparticles, especially at lower concentrations, with finer dispersion degrees leading to increased adhesion between the two phases.

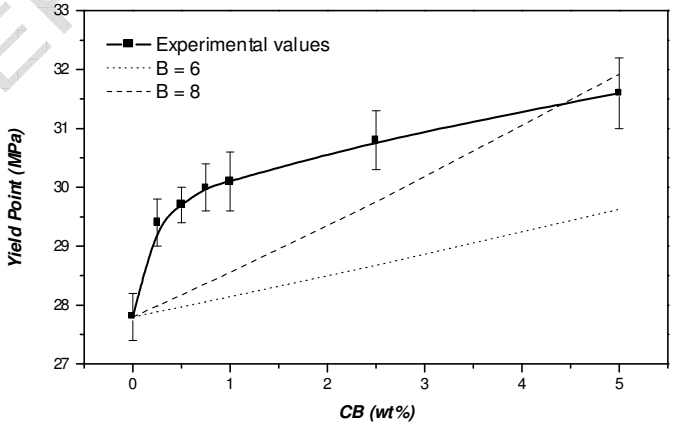

Figure 1. Tensile strength at the yield point of the prepared nanocomposites. The dashed lined indicate the corresponding theoretical trends according to Equation 1.

This calculated increase in adhesion between matrix and nanoparticles should also result in a higher tensile strength and Young's modulus of the prepared nanocomposites. However, as can be seen in Figure 2a tensile strength reduces by increasing the CN content. This behaviour is maybe due to the interactions between the nanoparticles themselves, as more and larger agglomerates are formed, which act as stress concentrators and ultimate failure points of the material [13, 17]. Generally, the drop in the tensile strength has been attributed to the reduction of the polymer fraction in the transverse cross-section of the polymer [27], which becomes an even greater issue due to the extremely large surface area of the filler used, and the presence of stress concentration around the filler's particles [28]. However, there are also reported that in some polymers like polyurethanes the tensile strength can increases by increasing the CN content [29], while the most characteristic example is rubber reinforced by CN, which results in increased Young's modulus and tensile strength [30]. In our case such enhancement in tensile strength was not achieved maybe due to the e aggregates than CN are formed into PP matrix. This was found out via microscopic and Raman observations and will be discussed latter.

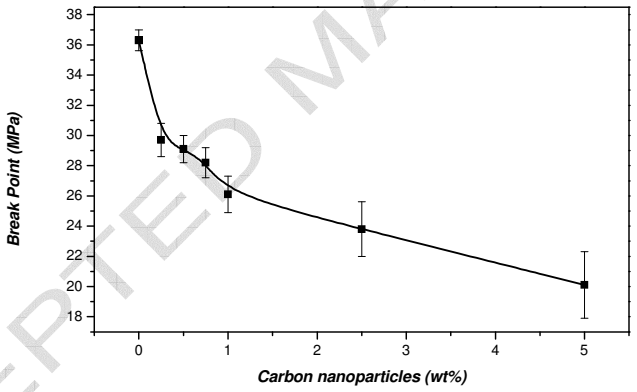

a

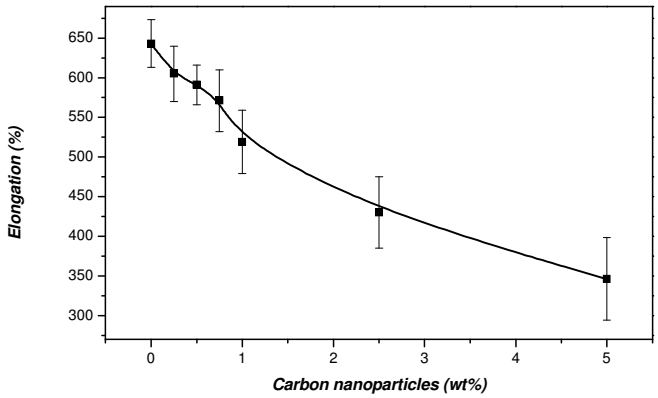

b

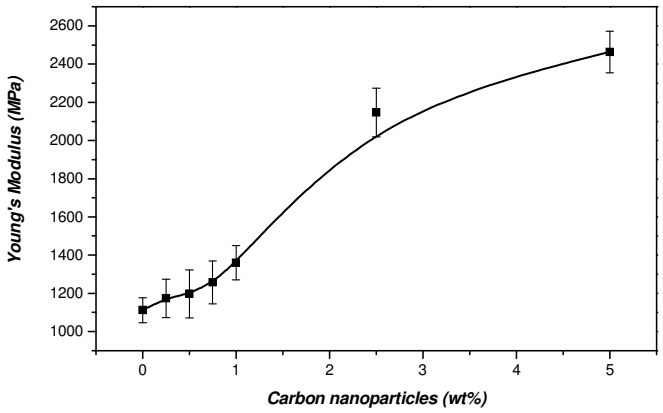

c

Figure 2. Experimental values of the prepared iPP/CN nanocomposites as a function of filler content of: a) Tensile strength at the break point b) Elongation at the break point c) Young's modulus.

The incorporation of filler in a thermoplastic polymer usually results in a decrease of the elongation at break, especially in the absence of any plasticizing effect. This was also observed in the prepared materials (Figure 2b). The finer the filler's dispersion, the smaller the reduction effect, since the size of the formed agglomerates is an important factor in determining their effectiveness to act as stress concentrators and ultimate failure points during extension. The trend in elongation decrease is similar to that observed for tensile strength. However, Young's modulus has a different trend from that recorded for tensile strength and gradually increases by increasing the CN content (Figure 2c). All the prepared nanocomposites presented significant improvement of Young's modulus with respect to pure iPP, even at 0.25 wt% CN. Increasing the concentration of the filler led to a further increase of the modulus, reaching a maximum improvement of 122 % for the sample containing 5 wt% CN, compared to the value obtained for the pure polymer (1.1 GPa).

3.2. Morphological characterization

Carbon black nanoparticles have the tendency to create agglomerations due to their high surface energy, since the Payne effect increases as the nanoparticles size decreases [31], as well as due to the existence of surface reactive groups. CN has a lot of surface functional groups which tend to interact with one other, creating large agglomerates. As reported very earlier by Rivin, carbon

black nanoparticles contain on their surface about 3 –OH groups and 0.05 –COOH per nm^2 [32]. In Figure 5 the TEM micrographs for iPP/CN containing 0.25 and 1 wt % CN are presented. As can be seen in nanocomposite containing 0.25 wt% CN these are dispersed into the PP matrix as individual particles in the range of 10-20 nm (Figure 3a). However, there are also some areas (not shown) where agglomerates up to 1 μm are formed. By increasing the CN content the agglomerate formation prevails and the relative amount of individual carbon nanoparticles is reduced (Figure 3b).

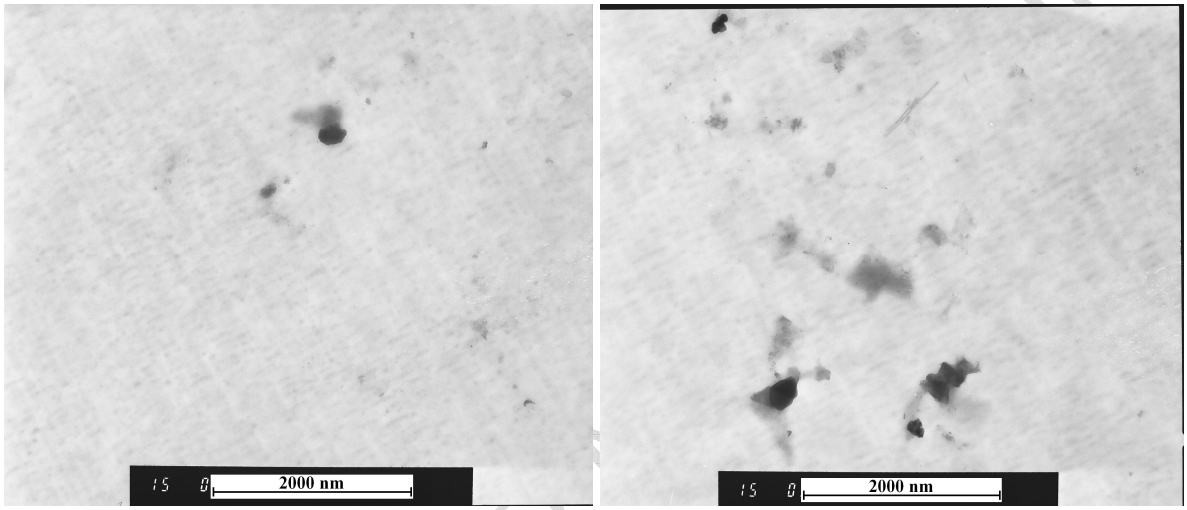

a **b**

Figure 3. TEM micrographs of the iPP/CN nanocomposites containing a) 0.25 wt% and b) 1 wt% CB nanoparticles.

Attempts to visualize these agglomerates with SEM were not successful. Therefore, in order to obtain an indication of the size of these larger structures as well as their possible size variation with CN concentration, micro-Raman spectroscopy was employed. Micro-Raman spectroscopy was used in previous studies of polypropylene composites [33] as well as on its nanocomposites to detect the thermal residual strains and chain orientation [34-36]. In the present work, 2D mapping of randomly selected areas of the composites is used for the visualization of the agglomerates and their distribution into the polymer matrix. Examination of the Raman spectra obtained for pure CN, neat iPP, and their composites with 0.5 and 5 wt% (Fig. 4a) showed that a broad band having a maximum intensity at 1594 cm^{-1} can be used for mapping concentration

variations of CN in the samples. This band is ascribed to the so-called "G band" (E_{2g2} vibration mode) of carbonaceous materials, which normally appears at 1582 cm^{-1}, and corresponds to the in-plane displacement of carbon atoms strongly coupled to hexagonal graphite sheets [37]. However, the broadening of this band in the present CN spectrum and the shifting of its maximum intensity to 1594 cm^{-1} (caused by its convolution with an additional, second-order, band at 1620 cm^{-1}), indicates the presence of significant disorder in the graphite lattice. The latter is also confirmed by the presence of another strong and equally broad band with an observed maximum centered at 1337 cm^{-1}, corresponding primarily to the A_{1g} vibrational mode of carbon atoms (also known as "D-band", typically having a maximum at app. 1350 cm^{-1} [38]).

The maps presented in Fig. 4 constitute plots showing the spatial variation of the intensity of the Raman signal at 1594 cm^{-1} on a plane approximately four microns below the samples' surface. The blue areas (low intensity) correspond to locations of low CN content, whereas the yellow and red indicate a strong signal produced by CN agglomerates. Areas of intermediate color, such as light blue and green, are taken to represent parts in the film where CN is present in fine dispersion within the iPP matrix. The results show that composites of low CN content (0.5 wt%; Fig. 4b) exist in relatively homogeneous dispersion and contain only small agglomerates with size less or equal to 2 microns. At higher CN content (5 wt%; Fig. 4c) larger agglomerates with sizes between 2 and 5 microns can be seen. Raman spectra acquired from composites with CN concentrations in the range 0.5-5 wt% (not shown here) also reveal a trend of increasing aggregate size with concentration. This phenomenon can offer an explanation for the reduced mechanical properties –tensile strength and elongation at break- exhibited by the nanocomposites with higher filler loadings. The agglomerates can act as points of mechanical failure inside a polymer matrix, thus behaving as usual fillers. In the case of iPP/CN the formation of CN agglomerates into iPP maybe unavoidable since, as showed from resent studies, carbon black nanoparticles have the tendency to create self assembled networks inside the polymers matrixes [39, 40].

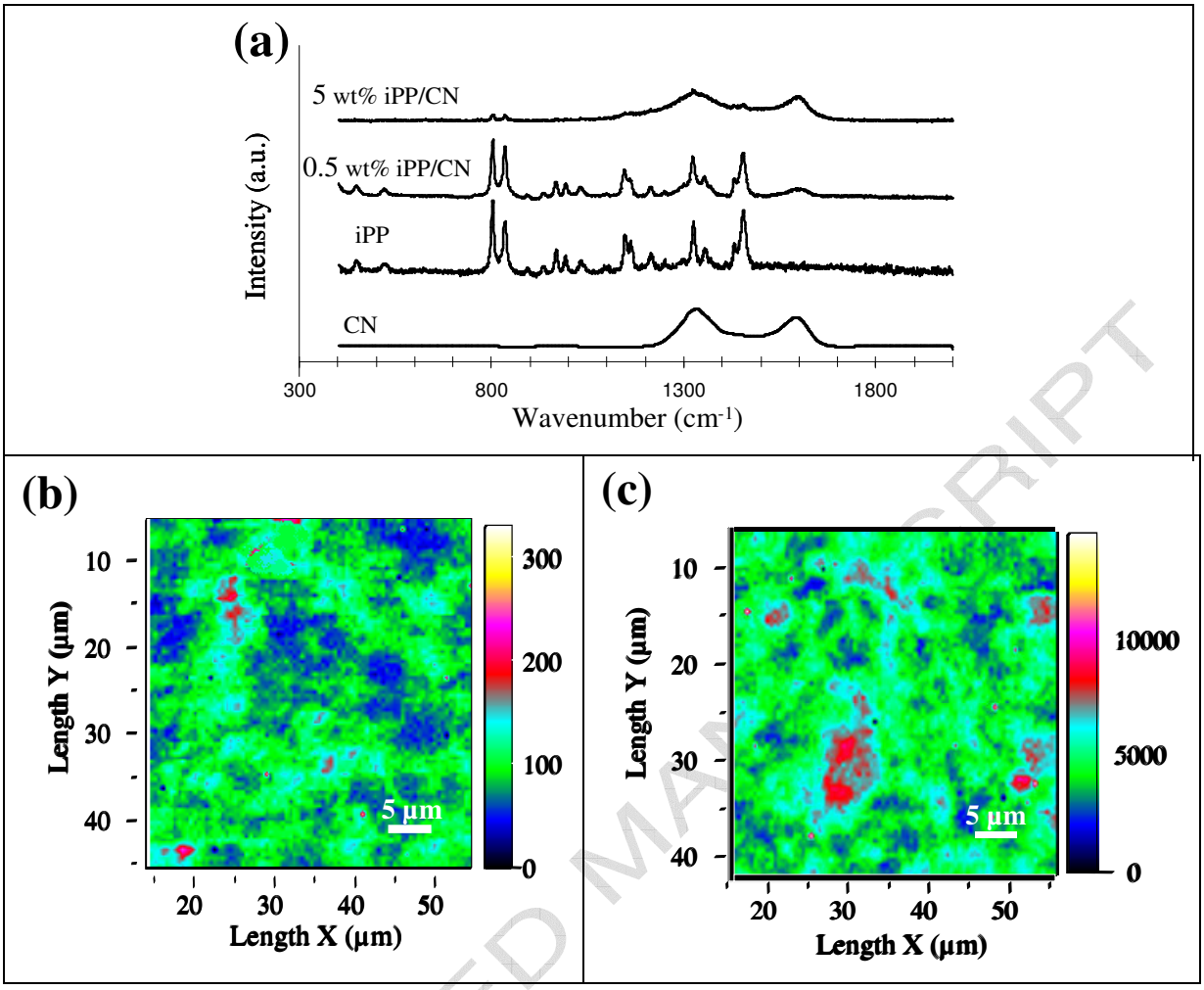

Figure 4. (a) Raman spectra of CN, neat iPP, and composites at 0.5 and 5 wt% CN content. (b) and (c) Micro-Raman maps from samples containing 0.5 wt% and 5 wt% CN, respectively. The colour bar indicates the intensity of the peak at 1594 cm^{-1}.

3.3. Effect of carbon black nanoparticles on iPP crystallization rate.

Nanoparticles are known from many studies to act as nucleating agents, enhancing the crystallization rate of polymers and the degree of their crystallinity [22]. Spherulite size and morphology are important factors in the characterization of iPP, since larger spherulites often promote brittleness owing to the concentration of structural defects and impurities at their boundaries. The spherulite morphologies of neat iPP and iPP containing 0.5 wt% CN under the optical microscope with crossed polarity are shown in Figure 5. In neat iPP many spherulites impinging on each other are found. The spherulitic sizes are greater than 30 µm and they are

complete. In the photograph of the nanocomposite containing 0.5 wt% CN large filler agglomerates are present. The size of these agglomerates increased with increasing filler content, in agreement with information found in the literature [13-16]. The spherulites' size, even with just 0.25 wt% CN content, is pronouncedly reduced (white spots in figure 5b) being barely observable and not exceed 0.5-1 μm in size. The iPP with CN nanoparticles shows much more spherulitic sites and a finer, grainy morphology. The carbon nanoparticles result in the formation of more iPP spherulites of much reduced size. That is expected since the nuclei density is much higher in the nanocomposites than that in pure iPP. When neighboring spherulite boundaries touch each other, they cease to propagate. As a result, the spherulite sizes will be reduced dramatically. Thus, the spherulites cannot be clearly observed. Comparing the two photographs we can conclude that CN acts as a nucleating agent, forcing iPP into less perfect and much smaller spherulites.

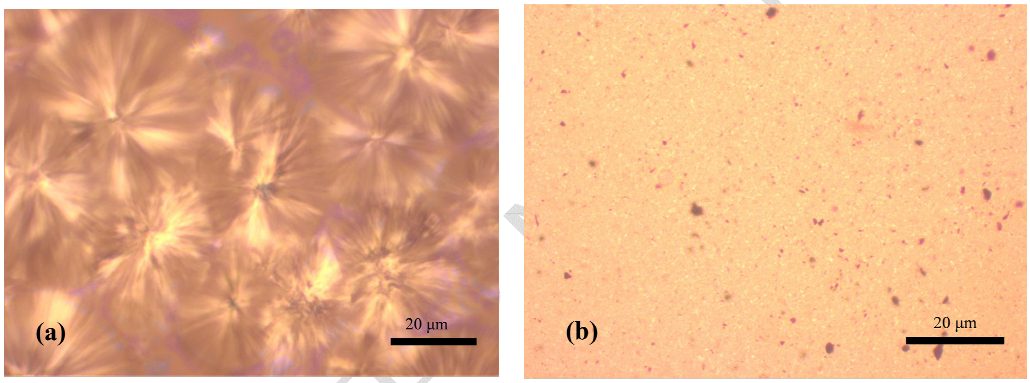

Figure 5. *POM* photographs taken during cooling at 10 $^{o}C \cdot min^{-1}$ of (a) pure iPP and (b) iPP containing 0.5 wt% CN nanoparticles.

The effect on CN on iPP crystallization was also studied with WAXD. Figure 6 shows the WAXD patterns of iPP and its nanocomposites in the range of 2θ, 10 to 25^{o}. The characteristic diffraction peaks of iPP at 13.9, 16.7, 18.3 and 21.6 ^{o} correspond to the planes (110), (040), (130) and (111) of its α-phase crystallite. The diffraction patterns of iPP/CN nanocomposites with CN content up to 2 wt% are found to be similar. However, in the nanocomposites containing 2.5 and 5 wt% CN an additional peak is recorded as a shoulder at 2θ = 19.27^{o}, which is attributed to the (130) plane of γ-phase crystallite of iPP, which consists of bilayers of two parallel helices with an inclination of 40 ^{o} to the lamellar surface [41].

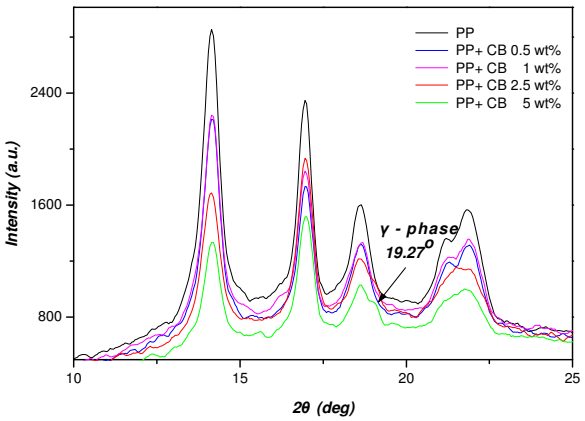

Figure 6. WAXD patterns of iPP/CN nanocomposites as received after melt mixing in the extruder.

It is well known that the addition of inorganic nanoparticles, such as SiO_2, can influence the nucleation of the polymer [18], however, the formation of the γ-phase iPP chainfolding is much more difficult [42]. Such chainfolding is only caused under isothermal crystallization at very high pressure and for iPP of very low molecular weight fractions. However, the formation of γ-phase was also reported in the case of intercalated iPP/clay nanocomposites prepared via melt mixing, whereat maleic anhydride was used as iPP modifier and an organophilic clay [43] but not in similar nanocomposites which contained exfoliated montmorillonite [44]. In the studied iPP/CN nanocomposites the CN nanoparticles are able to reduce the macromolecule's chain mobility, owing to the narrow space surrounding the dispersed CN nanoparticles. This reduction together with the nucleation effect of the CN nanoparticles, as found by *POM* observation, leads to the formation of smaller and less ordered crystallites (Figure 5b, POM). This phenomenon seems to be more intense in nanocomposites containing 2.5 and 5 wt% CN nanoparticles and, thus, γ-phase crystallites of iPP are also formed to a lesser extent.

3.4 Thermal Degradation

The effect of carbon nanoparticles on the thermal stability of the composites was studied by means of thermogravimetric experiments, carried out in both inert and oxidative conditions. In Figures 7-9, the mass loss (*TG* %) and the derivative mass loss (*DTG*) curves at a heating rate of 10^{o}C/min for the prepared samples in an atmosphere of N_2, O_2 and air are presented,

respectively. During the thermal degradation in inert atmosphere (N_2) all the samples present a single step degradation (Figure 7). Neat polypropylene begins to volatilise at about 270 ^{o}C, while the presence of carbon nanoparticles causes a shift of the initial weight loss towards higher temperatures. This shift is proportional to the amount of CN nanoparticles and, as can be followed, the maximum decomposition temperature (T_{max}) is reached for the i-PP/CN sample containing 5 wt% CN (~ 315 ^{o}C). Pure polypropylene degrades almost completely while the residues at the samples with carbon nanoparticles are directly related with the amount of CN nanoparticles added to iPP. Carbon nanoparticles also enhance the thermal stability of the samples at the onset degradation temperature (Table 1), which corresponds to an initial 2 % mass loss (T_d). Analogous behaviour of thermal stability in an inert atmosphere has been reported in the literature for iPP nanocomposites containing carbon nanotubes [45-48]. The stabilization effect of carbon nanoparticles could be explained by a barrier effect of the carbon nanoparticles, which hinders the diffusion of the degradation products from the bulk of the polymer to the gas phase. This labyrinth effect of carbon nanoparticles can be explained by comparing the degradation onset temperature shift with the corresponding maximum decomposition temperature of each nanocomposite. As can be seen from Table 1, in the nanocomposite containing 5 wt% CN the onset decomposition temperature is shifted to a higher temperature by about 40 ^{o}C while the maximum decomposition temperature (T_{max}) is only shifted by 10 ^{o}C [49, 50].

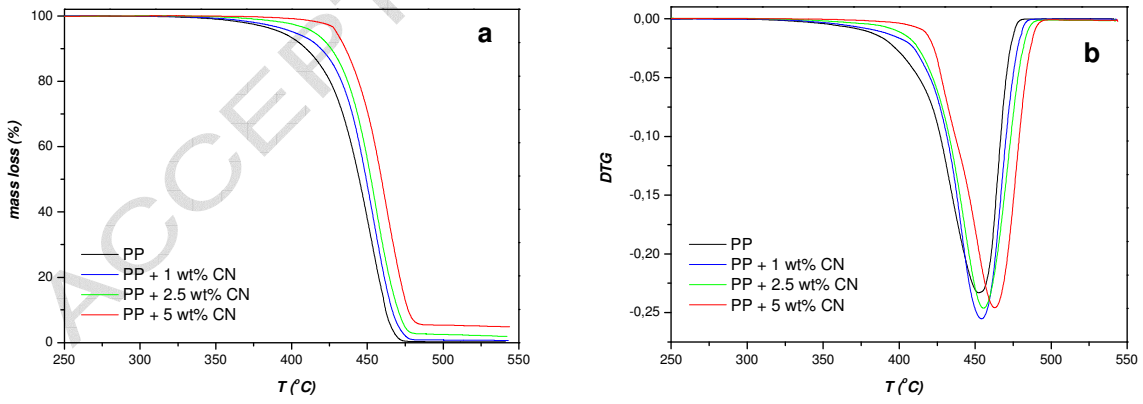

Figure 7. a) Mass loss (*TG%*) versus temperature for i-PP/CN nanocomposites containing different CN content and b) Derivative mass loss (*DTG*) versus temperature for i-PP/CN nanocomposites containing different CN content, under N_2 (heating rate β=10^{o}C/min).

Table 1. Characteristic thermal decomposition temperatures and remaining residue of iPP/CN nanocomposites under different atmospheres.

Sample	Onset (°C)	Endset (°C)	T_{max} (°C)	T_d (°C)	Residue %
Carrier gas N_2					
Ipp	273.6	500.0	452.3	368.0	0.2
iPP + 1 wt% CN	280.8	500.9	454.3	375.3	0.7
iPP + 2.5 wt% CN	285.4	504.1	455.6	394.6	1.9
iPP + 5 wt% CN	315.6	504.9	462.8	418.6	4.8
Carrier gas O_2					
iPP	212.8	380.0	295.9	237.7	4.7
iPP + 1 wt% CN	192.8	375.8	299.8	226.2	9.8
iPP + 2.5 wt% CN	181.5	375.6	344.5	215.7	10.8
iPP + 5 wt% CN	182.4	375.3	353.2	221.0	11.2
Carrier gas *Air*					
iPP	226.9	415.3	362.7	265.7	2.4
iPP + 1 wt% CN	211.9	424.8	391.3	258.1	3.0
iPP + 2.5 wt% CN	200.2	434.8	397.8	257.9	4.6
iPP + 5 wt% CN	203.5	460.5	409.7	261.4	7.0

The thermo-oxidative degradation of neat isotactic polypropylene under O_2 takes place in two distinct stages from 200 to 410 °C (Figure 8). The first stage appears at temperatures up to 312°C and corresponds to a mass loss of about 92% while the second is presented between 312 and 475°C, where the remaining mass of iPP is degraded. Moreover, the influence of carbon nanoparticles under oxidative atmosphere is not analogous to that recorded under an inert atmosphere. As can be seen from all the thermograms, as well as from Table 1, the carbon nanoparticles reduce the thermo-oxidative stability of *i-PP*. The thermogravimetric profile of the nanocomposites is more complex, showing more than two decompositions stages, as is more clearly depicted by the *DTG* curves. The temperatures at which degradation starts in all nanocomposites and the temperatures corresponding to initial 2% of mass loss (T_d) are shifted to lower values by increasing CN content up to 2.5 wt%. After that concentration the degradation behaviour remains unaffected. Characteristically, while the decomposition of iPP starts at 330°C the corresponding temperature for the sample containing 5 wt% CN is 30 °C lower (300°C). It seems that the carbon nanoparticles play an accelerating role at the beginning of polymer decomposition. Such an accelerating behaviour at the first stages of iPP decomposition was also

mentioned for iPP/carbon nanotubes nanocomposites [51]. In literature many explanations have been reported in order to explain this phenomenon, and most of them are attributing this accelerating effect to the remaining traces of inorganic elements, such as *Fe* and *Co* [52, 53]. However, the precise mechanism and the released by-products at this stage are not well documented, thus necessitating further and more precise study. Furthermore, in our used nanoparticles such elements were not detected. By the end of this stage, the effect of CN upon the maximum decomposition temperature (T_{max}) is analogous to that observed under an inert atmosphere and increases with CN content. Furthermore, the residue was larger than under inert atmosphere at the respective temperatures.

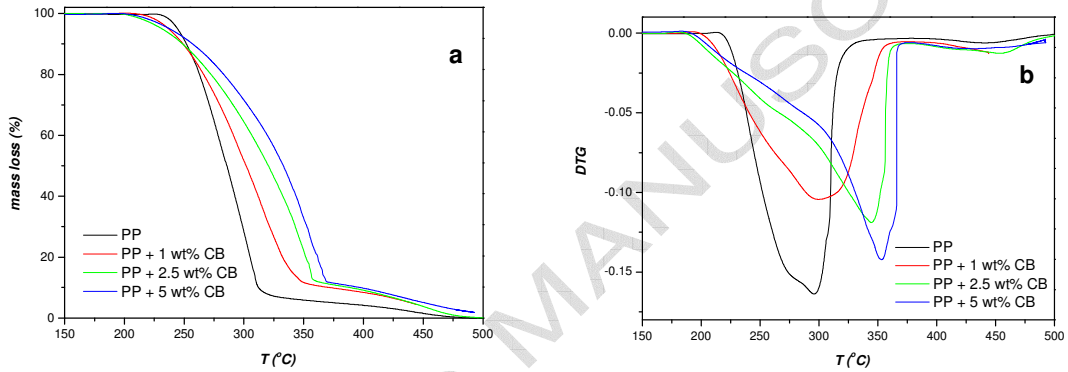

Figure 8. a) Mass loss (*TG%*) versus temperature for *i-PP*/CN nanocomposites containing different CN content and b) Derivative mass loss (*DTG*) versus temperature for *i-PP*/CN nanocomposites containing different CN content under O_2 (heating rate β=10°C/min).

The degradation behaviour of the prepared nanocomposites under air (Figure 9) was between that observed under an inert atmosphere and O_2. As seen in Figure 9a, the decomposition of iPP and its nanocomposites initiated at similar temperatures, 247 and 232°C respectively, with very small differences between them. Thus, neither the accelerating behaviour, recorded in O_2, nor the stabilization effect of CN nanoparticles, recorded in N_2, was observed. The temperature at which decomposition of the iPP/CN nanocomposites initiates is very crucial, since most iPP products are industrially prepared at temperatures close to 200 °C and, thus, it should be concluded that thermal oxidation can be avoided. Two stages of mass loss can be identified, mainly for the samples containing CN, as seen from the shoulder recorded in the *DTG* peak (Figure 9b).

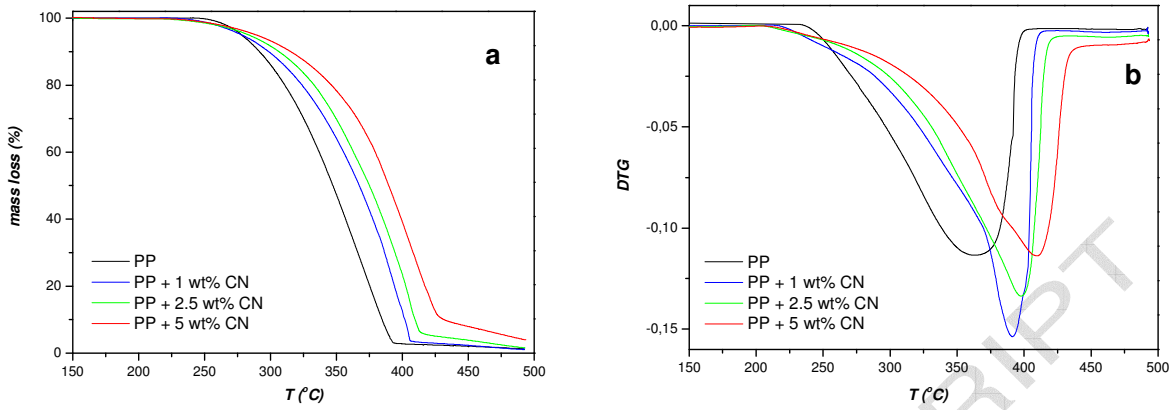

Figure 9. a) Mass loss (*TG%*) versus temperature for *i-PP*/CN nanocomposites containing different CN content and b) Derivative mass loss (*DTG*) versus temperature for *i-PP*/CN nanocomposites containing different CN content under air (heating rate β=10°C/min).

3.4 Gas transmission rates

The presence of a filler, inorganic or organic, in the polymer matrix usually constitutes a solid barrier in the path of the gas molecules passing through the polymer. A more tortuous path is thus forced upon the gas molecules passing through the polymeric matrix, retarding the progress of the phenomenon. The more tortuous the path the longer it takes for the gas molecules to pass through the material, resulting in a macroscopically observed reduced permeability. The higher the filler-matrix interfacial area and aspect ratio of the filler, the more tortuous the path, hence the greater the decrease in permeability. This is the reason why nanocomposites are vigorously examined for their permeability rates' enhancements, due to their high interfacial area, and mostly in polymer/layered silicate nanocomposites, due to the high aspect ratio of the filler [54]. Although spherical carbon nanoparticles are not considered the most effective barrier, as in the case of sheet-like layered silicates, where due to their high length-to-width ratio the path length of the gas is maximized, nonetheless such nanoparticles should also significantly reduce gas diffusion through the material. Thus, the permeability rates of N_2, O_2. and CO_2 through thin films of the prepared iPP/CN nanocomposites were measured to evaluate the enhancement effect of the carbon nanoparticles' addition.

The gas transmission rates (*TR*) through a thin film of each iPP/CN nanocomposite sample were calculated using the following equation, according to the apparatus's instructions:

$$TR = \frac{(273\ p\ V)(24\,10^4)}{A\ T\ P} \qquad (2)$$

where *TR* is the gas transmission rate (ml/m^2 · day · atmosphere), *p* is the rate of pressure change in the capillary pipe (cm Hg/h), *V* is the total free volume in the sample shell (5 ml), *A* is the surface of the sample (23.77 cm^2), *T* is the temperature at which the experiment is carried out (25^{o}C) and *P* is the pressure difference at the beginning of the experiment in cm Hg which can be considered equal to 76 cm Hg.

Transmission rates are easily converted to gas permeability by the following equation:

$$\boldsymbol{P = (TR)\,l} \qquad (3)$$

where *l* is the film's thickness (cm).

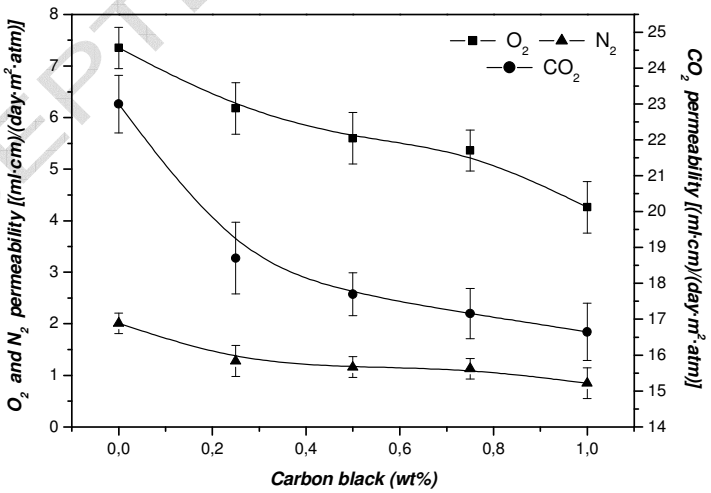

Figure 10. Permeability of N_2, O_2 and CO_2 gases of iPP/CN nanocomposites as a function of filler content.

The permeabilities of all three gases are reduced to an unexpectedly significant extent, as the carbon nanoparticles' content is increased, reaching a maximum reduction of 28 % for CO_2, 42 % for O_2 and 58 % for N_2, as seen in Figure 10. The matrix used is a semi-crystalline polymer and it consists of crystalline and amorphous regions. The crystalline regions are considered impenetrable regions by gases and, thus, gas molecule diffusion is only through the amorphous phases. The existence of different phases in nanocomposites can cause complex phenomena over the process of gas permeation. Because carbon nanoparticles can act as nucleating agents, the degree of crystallinity (as was measured by DSC) ranges from 62 for the neat iPP up to 67% for the nanocomposite containing 5 wt% CN. Thus, it is possible the lower permeabilities for the samples containing higher CN content are due to the higher crystallinity. Furthermore, the presence of micro-crystalline carbon nanoparticles forces the gas molecules to follow a much more complicated path in order to pass through the film. These more tortuous paths, which are proportional to the specific surface of the filler, contribute in the observed penetrability reduction. Thus, apart from the matrix's crystalline regions the gas molecules need also to by-pass the micro-crystalline carbon nanoparticles, which are considered impenetrable by them. Carbon black is an active strengthening material; its effect is becomes more pronounced with increasing specific surface area and/or surface energy. Carbon black particles are composed of a large number of agglomerated crystalline elements, called microcrystallites. In general, the system of microcrystallites in a carbon black particle is concentric and the particles are in the shape of spheres or agglomerated spheres which form less or more extended spatial chains [4]. So, it is also possible these nanocrystallites containing in the carbon nanoparticles to contribute to a further reduction of gas permeability.

By comparing the permeability rates of the three gases examined it becomes obvious that CO_2 has the highest permeability while N_2 the lowest. This behaviour is mostly attributed to the significantly different solubility of each gas in isotactic polypropylene. The Henry's law coefficients for CO_2, N_2 and O_2 in iPP at 25 ^{o}C are 42.2×10^{-4}, 3.40×10^{-4} and 6.60×10^{-4} cm^3 $(STP)/cm^3$(polym)cmHg, respectively [55]. Especially in the case of CO_2, the diffusion is also influenced by the gas concentration in the polymer, since there is a plasticizing effect of the penetrant on diffusion. The gas enters the polymer and enlarges the matrix, so that segmental motion and hence gas diffusion are accelerated [56]. Furthermore, in the case of O_2 and N_2, the

different diameters of the gases also have to be considered. These were found from the literature to be equal to 3.64 and 3.46 Å for nitrogen and oxygen, respectively. The lower kinetic diameter implies that oxygen can pass more easily through the nanopores of the polymeric matrix. Considering all the above, the different permeability rates can be sufficiently interpreted.

4. Conclusions

Carbon nanoparticles, synthesizes by a shock wave propagation method from the free carbon of the explosive, are finely dispersed in isotactic polypropylene using a twin screw co-rotating extruder. This led to a significant enhancement of the material's Young's modulus, as well as to a small improvement of the tensile strength at the yield point. However, micro-Raman spectroscopy and TEM micrographs reveal that some agglomerates also form in sizes approximately 2-5 μm, which slightly deteriorate the tensile strength and elongation at the break point by increasing the filler's concentration. The nanoparticles act as nucleating agents but cause also a significant reduction of the iPP chain's mobility, resulting in the formation of much smaller and less ordered crystallites. In inert atmosphere thermal stability of iPP matrix is substantially improved (N_2) due to the presence of the nanoparticles, while under oxygen thermal decomposition is more complex, displaying more than two stages. In air, the degradation behaviour lies between those exhibited in N_2 and O_2 atmospheres. Permeability rates for the gases measured are substantially lowered with increasing filler content, up to 28 % for CO_2, 42 % for O_2, and 58 % for N_2 at a filler concentration of just 1 wt% CN.

5. References

[1] Gächter R, Müller H, (Eds.). Plastics Additives Handbook, Hanser Publishers, Munich, 1990.
[2] Huang JC, Adv Polym Techn 2002; 21: 299.
[3] Sichel EK, Editor. Carbon black polymer composites. New York: Marcel Dekker, 1989.
[4] Koszkul J. Energochemia, Ekologia, Karbo 1997; 42: 84.
[5] Bikiaris DN, Achilias DS, Giliopoulos DJ, Karayannidis GP. Eur Polym J 2006; 42: 3190.
[6] Allen NS, Edge M, Corrales T, Childs A, Liauw CM, Catalina F, Peinado C, Miniham A, Aldcroft D. Polym Degrad Stab 1998; 61: 183.
[7] Mwila J, Miraftab M, Horrocks AR. Polym Degrad Stab 1994; 44: 351.
[8] Jakab E, Omastová M. J Anal Appl Pyrolysis 2005; 74: 204.
[9] Horrocks AR, Mwila J, Miraftab M, Liu M, Chohan SS. Polym Degrad Stab 1999; 65: 25.
[10] Blanco A. Plast Eng, May 2000; 40.
[11] Mucha M, Marszałek J, Fidrych A. Polymer 2000; 41: 4137.
[12] Tjong SC. Mater Sci Eng 2006; R 53: 73.

[13] Bikiaris DN, Papageorgiou GZ, Pavlidou E, Vouroutzis N, Palatzoglou P, Karayannidis GP. J Appl Polym Sci 2006; 100: 2684.
[14] Vladimirov V, Betchev C, Vassiliou A, Papageorgiou G, Bikiaris D. Comp Sci Techn 2006; 66: 2935.
[15] Kontou E, Niaounakis M. Polymer 2006; 47: 1267.
[16] Liu Y, Kontopoulou M. Polymer 2006; 47: 7731.
[17] Bikiaris DN, Vassiliou A, Pavlidou E. Karayannidis GP. Eur Polym J 2005; 41: 1965.
[18] Papageorgiou GZ, Achilias DS, Bikiaris DN, Karayannidis GP. Therm Acta 2005;427:117.
[19] Lee JA, Kontopoulou M, Parent SJ. Macromol Rapid Comm 2007; 28: 210.
[20] Bikiaris DN, Karavelidis V, Karayannidis GP. Macromol Rapid Comm 2006; 27: 1199.
[21] Plummer CJG, Garamszegi L, Leterrier Y, Rodlert M, Manson JAE. Chem Mater 2002; 14: 486.
[22] Vassiliou AA, Papageorgiou GZ, Achilias DS, Bikiaris DN. Macrocol Chem Phys 2007; 208: 364,
[23] Chrissafis K, Antoniadis G, Paraskevopoulos KM, Vassiliou A, Bikiaris DN. Comp Sci Techn 2007; 67: 2165..
[24] Jain S, Goossens H, Picchioni F, Magusin P, Mezari B, van Duin M. Polymer 2005; 46: 6666.
[25] Stavrev S. U.S. Patent 5353708, 1994.
[26] Turcsányi B, Pukánszky B, Tüdõs F. J Mater Sci Lett 1988; 7: 160.
[27] Nielsen LE. J Appl Polym Sci 1996; 10: 97.
[28] Sahu S, Broutman LJ. Polym Eng Sci 1972; 12: 91.
[29] Hwang J, Muth J, Ghosh T. J Appl Polym Sci 2007; 104: 2410.
[30] Medalia AI, Kraus G, 'Reinforcement of Elastomers by Particulate Fillers, in Science and Technology of Rubber'. Mark JE, Erman B, Eirich FR, Eds., Academic, New York 1994.
[31] Hess WM, Vegvari PC, Swor RS. Rubber Chem Technol 1989; 58: 350.
[32] Rivin D. Rubber Chem Tech 1971; 44: 307.
[33] Tselios Ch, Bikiaris D, Savidis P, Panayioyou C. J Mater Sci 1999; 34: 385.
[34] Nielsen AS, Pyrz R. Polym Polym Comp 1997; 5: 245.
[35] Thomsen JS, Pyrz R. Comp Sci Techn 1999; 59: 1375.
[36] García-López D, Merino JC, Pastor JM. J Appl Polym Sci 2003; 88: 947
[37] Knight DS, White WB. J Mater Res 1989; 4: 385.
[38] Wang Y, Alsmeyer DC, McCreery RL. Chem Mater 1990; 2: 557
[39] Koshini Y, Cakmak M. Polymer 2006; 47: 5371.
[40] Bandyopadhyaya R, Rong W, Friedlander SK. Chem Mater 2004; 16: 3147.
[41] Meille S, Bruckner S, Porzio W. Macromolecules 1990; 23: 4114.
[42] Thomann R, Semke H, Maier RD, Thomann Y, Scherble J, Mulhäupt R, Kressler J. Polymer 2001; 42: 4597.
[43] Nam PH, Maiti P, Okamoto M, Hasegawa N, Usuki A. Polymer 2001; 42: 9633.
[44] He A, Wang L, Li J, Dong J, Han CC. Polymer 2006; 47: 1767.
[45] Zanetti M, Camino G, Reichert P, Mulhaupt R. Macromol Rapid Comm 2001; 22: 176.
[46] Tang Y, Hu Y, Song L, Zong R, Gui Z, Chen Z. Polym Degrad Stab 2003 ; 82: 127.
[47] Qin H, Zhang S, Zhao C, Feng M, Yang M, Shu Z. Polym Degrad Stab 2004; 85: 807.
[48] Vyazovkin S, Sbirrazzuoli N. Macromol Rapid Comm 2006; 27: 1515.
[49] Yang J, Lin Y, Wang J, Lai M, Li M, Liu J, Tong X, Cheng H. J Appl Polym Sci 2005; 98: 1087.

[50] Chatterjee A, Deopura BL. J Appl Polym Sci 2006;100: 3574.
[51] Sarno M, Gorrasi G, Sannino D, Sorrentino A, Ciambelli P, Vittoria V. Macromol Rapid Comm 2004; 25: 1963.
[52] Hirschler MM. Polymer 1984; 25: 405.
[53] Carty P, White S. Fire Safety 1994; 23: 67.
[54] Ray S, Yamada K, Okamoto M, Ogami A, Ueda K. Chem Mater 2003; 15: 1456.
[55] Naito Y, Mizoguchi K, Terada K, Kamiya Y. J Polym Sci Part B Polym Phys 1991; 29: 457.
[56] Kamiya Y, Mizoguchi K, Hirose T, Naito Y. J Polym Sci Polym Phys Ed 1989; 27: 879.